Supplementary Information

Greater North American Monsoon Precipitation Brought by Enhanced Storm Activity in a Warm Climate

Supplementary Figures 1 to 15

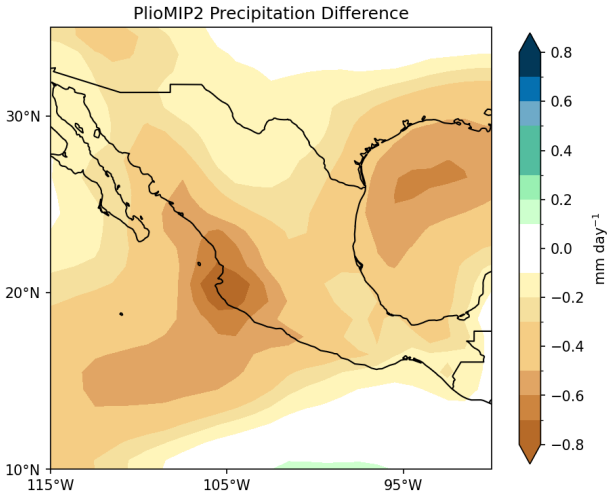

Supplementary Fig. 1 June–September precipitation differences between the PlioMIP2 ensemble mean and the preindustrial control runs. Positive (negative) MP–PI values indicate wetter (drier) conditions than PI.

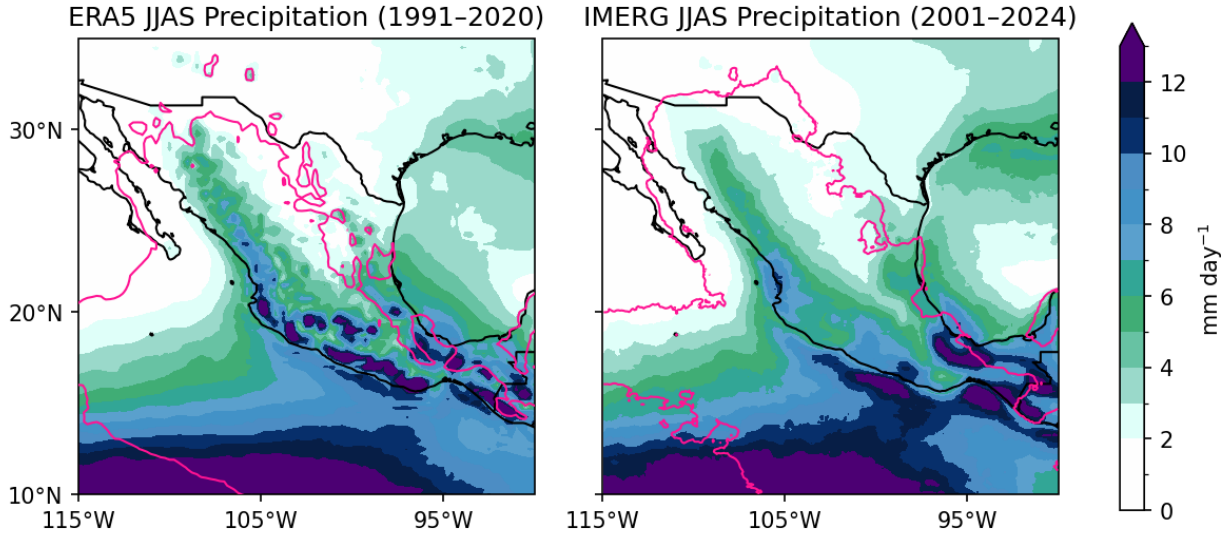

Supplementary Fig. 2 Average June–September precipitation in ERA5 (left) between 1991–2020 and IMERG (right) between 2001-2024. Pink contours are core monsoon extent. We define the monsoon here as summer precipitation (JJAS) exceeding 60% of the annual total.

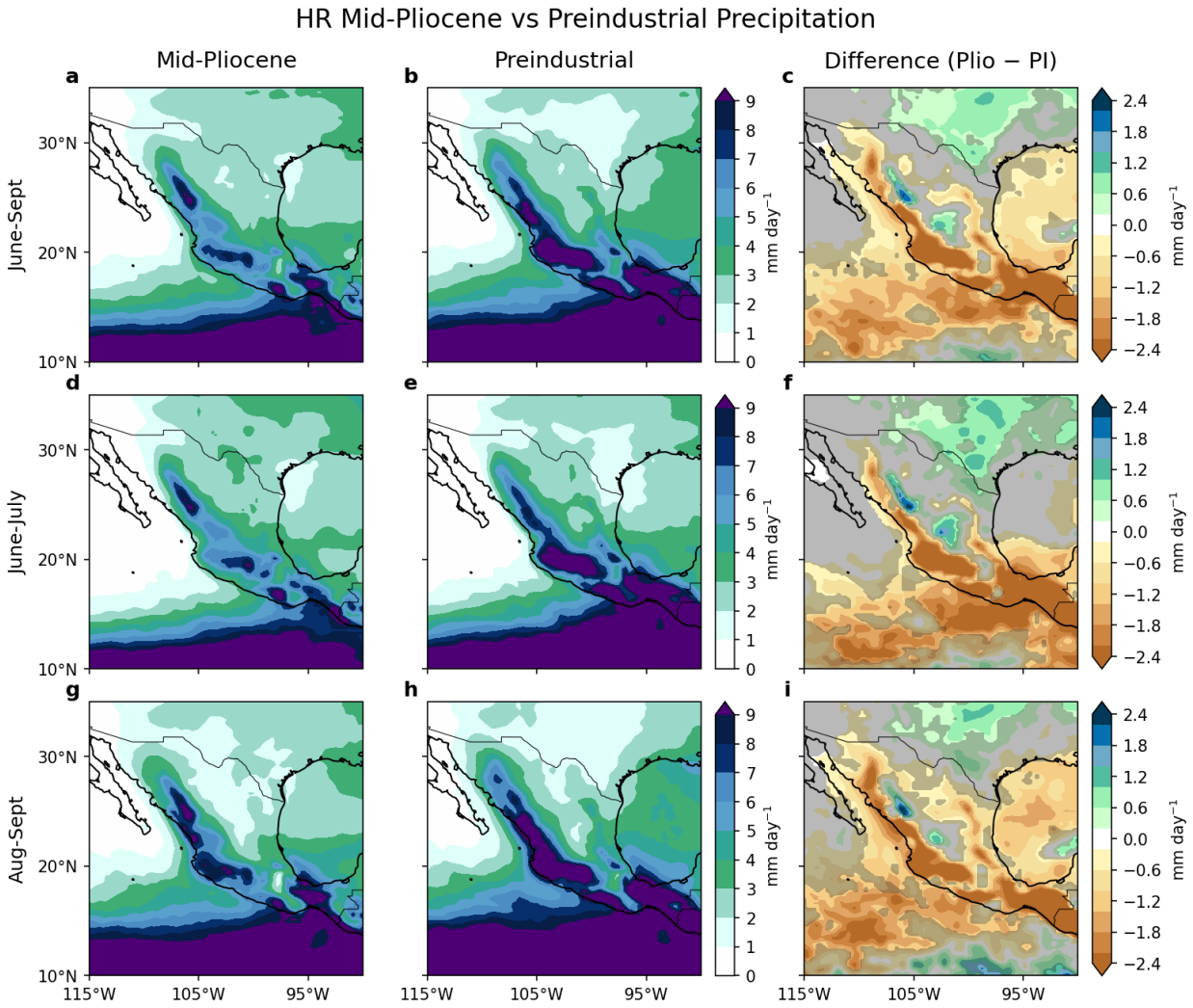

Supplementary Fig. 3 High-resolution mid-Pliocene and Preindustrial monthly-mean precipitation (left and middle columns) and their differences (right column) for JJAS (top), JJ (middle), and AS (bottom), averaged over the selected simulation years. Differences (Plio PI) are shaded in gray where the change is not statistically significant ($p \geq 0.05$; two-sided Welch t-test). All values are shown in mm day^{-1}.

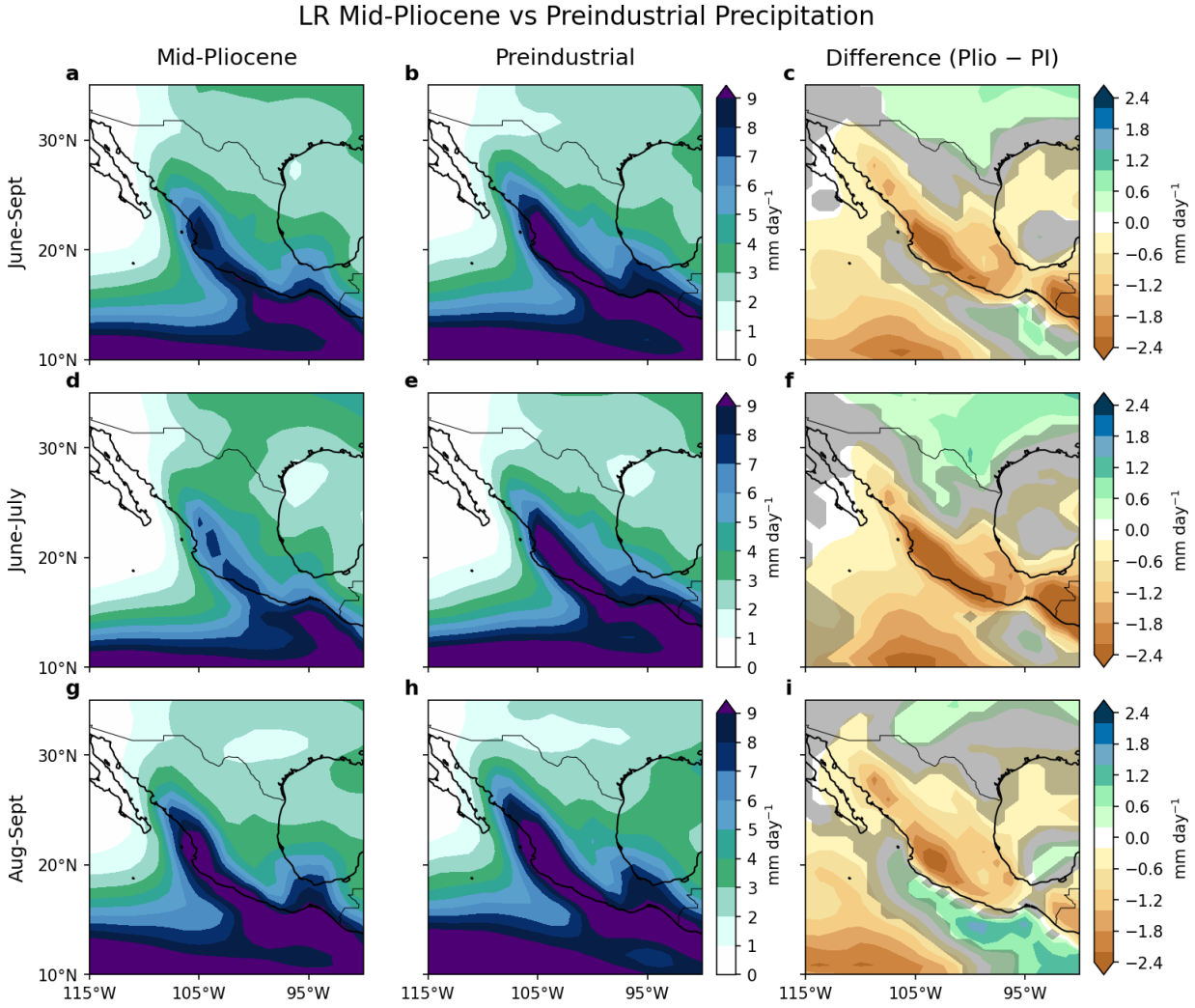

Supplementary Fig. 4 Same as Supplementary Figure 3, but for low-resolution.

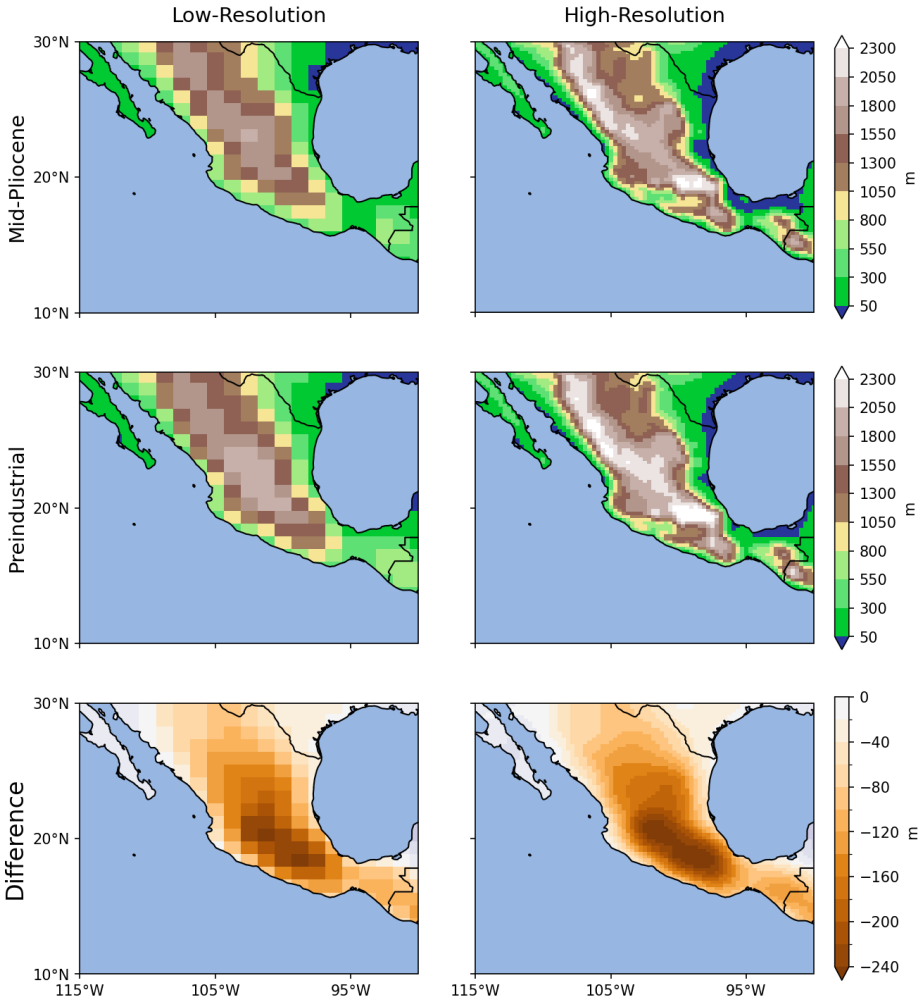

Supplementary Fig. 5 Low-resolution (left) and high-resolution (right) elevation for mid-Pliocene (top) and preindustrial (middle) simulations and their difference (bottom).

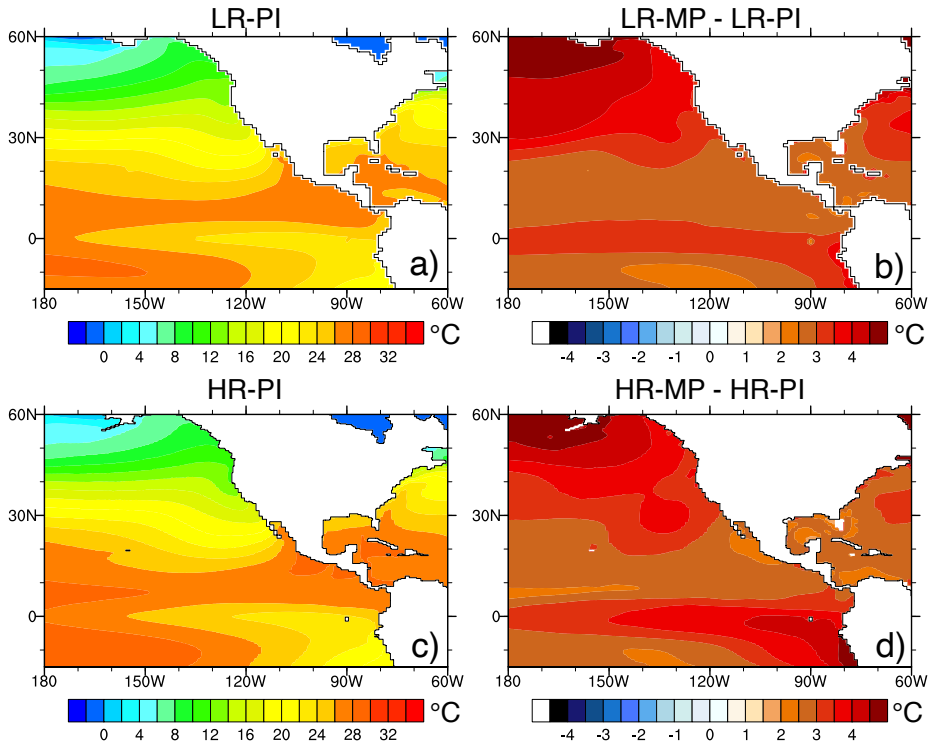

Supplementary Fig. 6 Simulated preindustrial SST in (a) LR and (c) HR runs and the difference between MP and PI in (c) LR and (d) HR simulations.

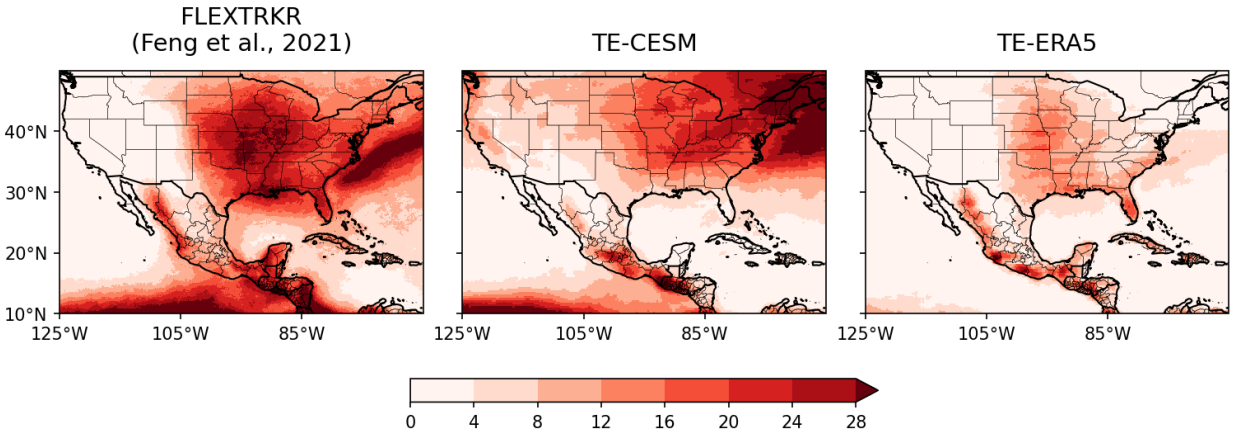

Supplementary Fig. 7 Average number of MCSs per March–August season over the CONUS. FLEXTRKR on radar data (Feng et al., 2021) (left). TempestExtremes on a historical (1991-2003) CESM simulation (middle) and TempestExtremes on ERA5 (1991-2003; right).

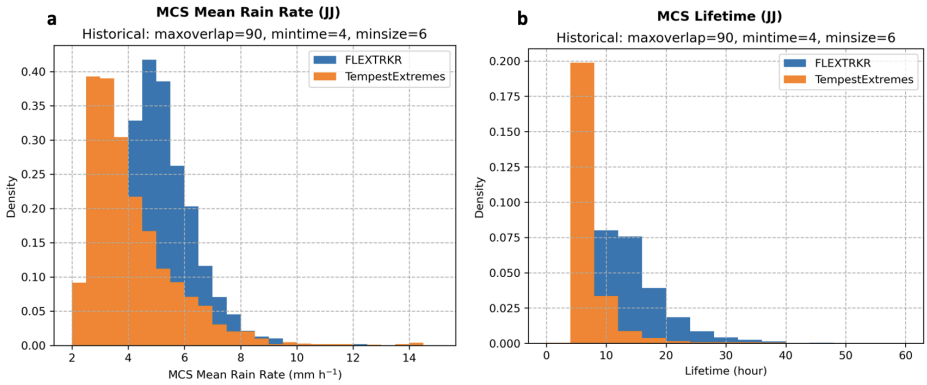

Supplementary Fig. 8 Comparison of MCS stats using TempestExtremes with historical CESM simulation to FLEXTRKR from Feng et al. (2021).

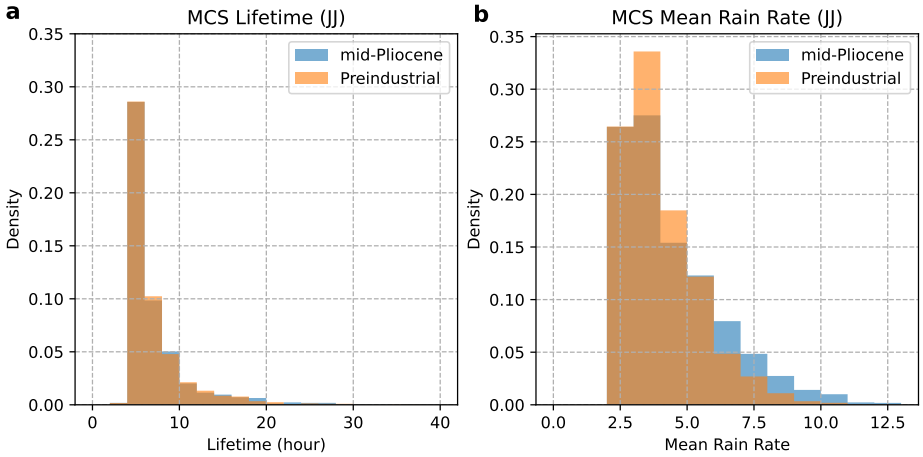

Supplementary Fig. 9 Comparison of June-July MCS lifetime (a) and mean rain rate (b) in HR-MP and HR-PI.

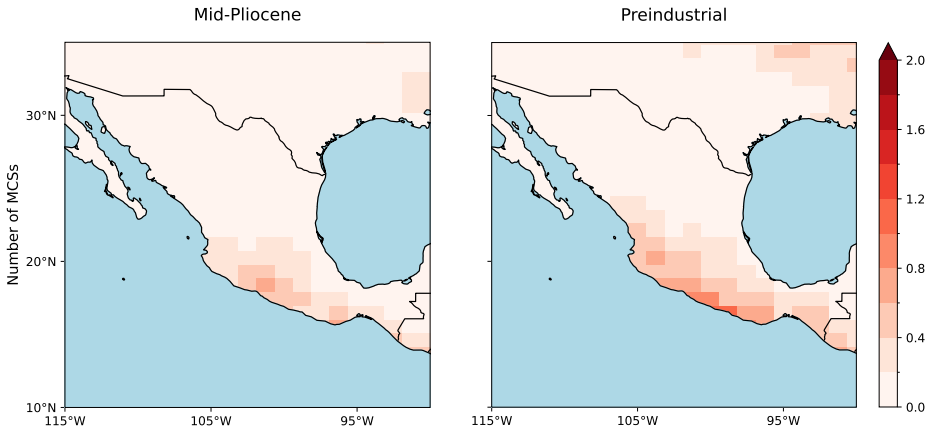

Supplementary Fig. 10 Average number of MCSs per June–July season in low-resolution simulations.

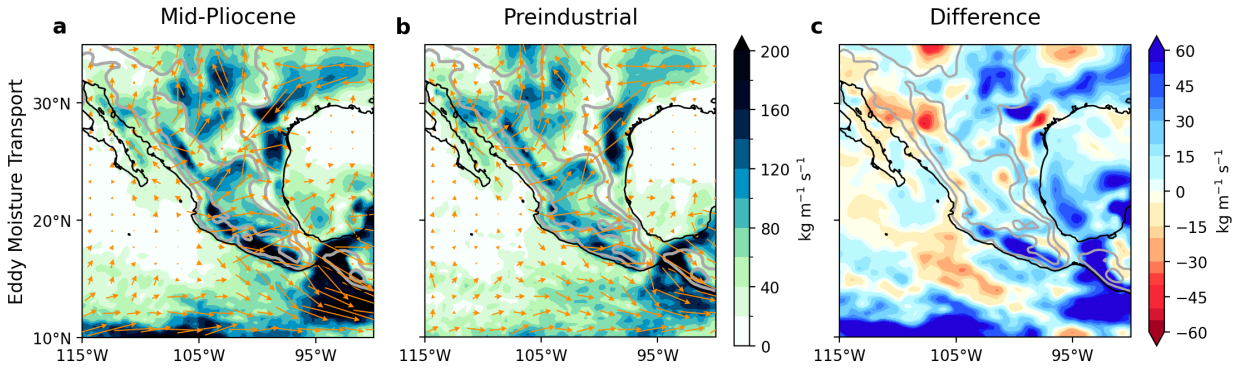

Supplementary Fig. 11 Magnitude of eddy moisture transport (shading) with vectors of actual transport integrated through the atmospheric column from the surface for the mid-Pliocene (a) and preindustrial (b). Difference between mid-Pliocene and preindustrial in actual moisture transport (c). Grey contours in (a–c) are topography at 1000 m intervals, starting at 500 m.

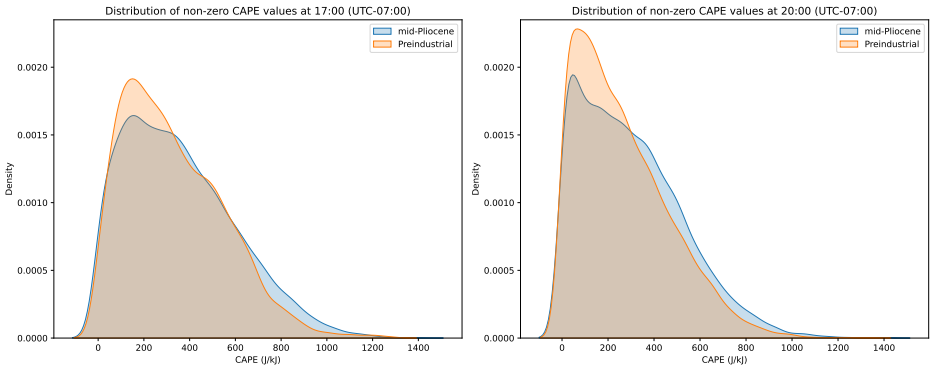

Supplementary Fig. 12 Comparison of CAPE in HR-MP and HR-PI for 17:00 (left) and 20:00 (right) local time within 25°N–27°N, 105°W–106°W.

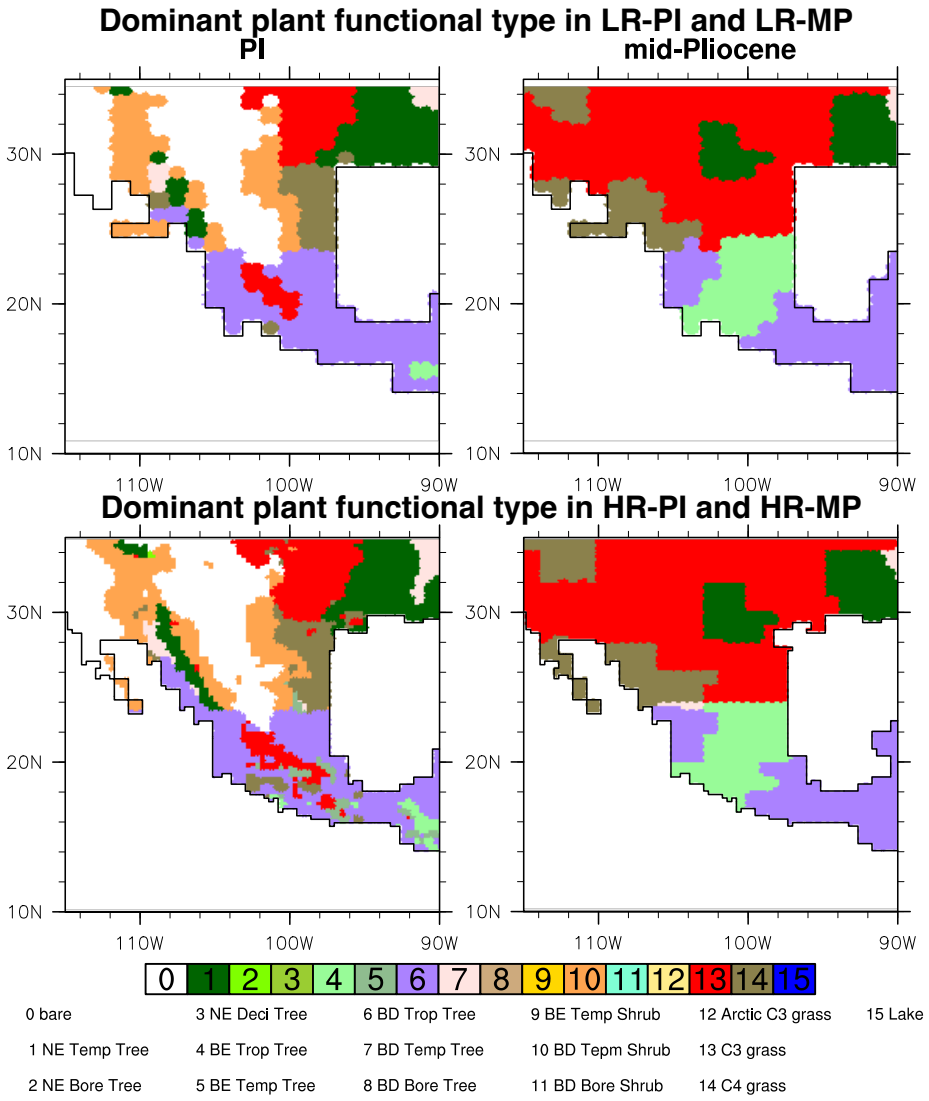

Supplementary Fig. 13 Dominant plant functional types for PI (left column) and MP (right column) in LR (top panel) and HR (bottom panel).

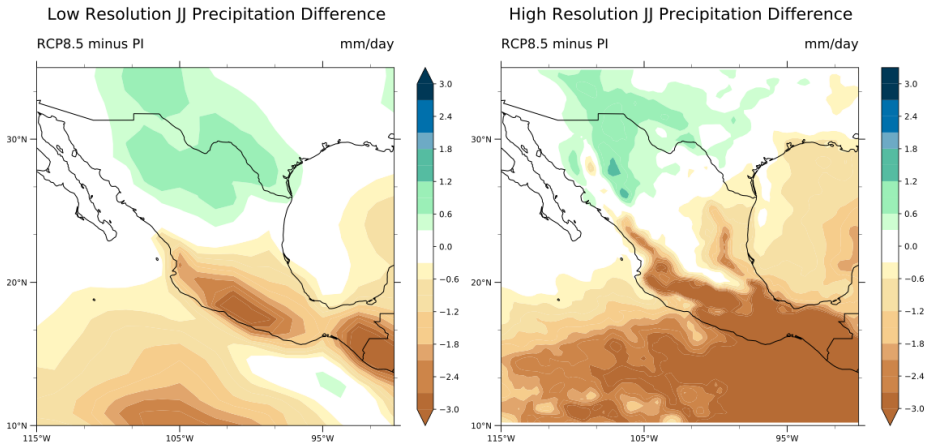

Supplementary Fig. 14 Early summer (June-July) precipitation differences between HighResMIP RCP8.5 CESM run and preindustrial control in (left) low- and (right) high-resolution.

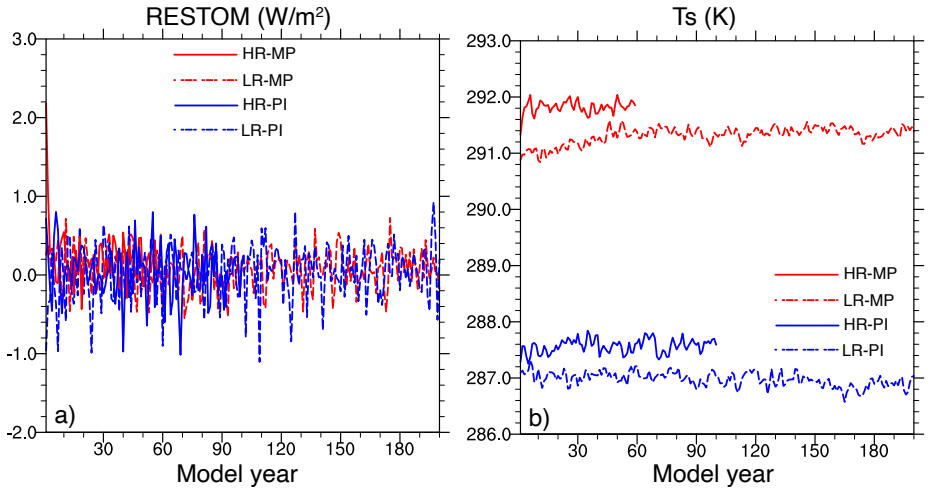

Supplementary Fig. 15 Diagnostics of equilibrium states of high-resolution (HR) and low-resolution (LR) simulations: (a) top-of-atmosphere radiation imbalance and (b) global-mean surface temperature.